

Radiolabeled Neuronal Nitric Oxide Synthase Inhibitors: Synthesis, In Vivo Evaluation, and Primate PET Studies

Martin G. Pomper, John L. Musachio, Ursula Scheffel, James E. Macdonald, Dennis J. McCarthy, David W. Reif, Victor L. Villemagne, Fuji Yokoi, Robert F. Dannals, and Dean F. Wong

Department of Radiology, Johns Hopkins University School of Medicine, Baltimore, Maryland; and Astra Arcus U.S.A., Rochester, New York

The objectives of this study were to synthesize neuronal nitric oxide synthase (NOS-I)-selective imaging agents based on the 2 potent, selective inhibitors AR-R 17443 [*N*-(4-((2-((phenylmethyl) (methyl)-amino)ethyl)phenyl)-2-thiophenecarboximidamide)] and AR-R 18512 [*N*-(2-methyl-1,2,3,4-tetrahydroisoquinoline-7-yl)-2-thiophenecarboximidamide)] in positron-emitting form and to evaluate regional brain uptake in rodents and primates. **Methods:** [^{11}C]AR-R 17443 and [^{11}C]AR-R 18512 were produced by *N*-alkylation of the corresponding desmethyl precursors using [^{11}C]iodomethane. Regional brain uptake of [^{11}C]AR-R 17443 and [^{11}C]AR-R 18512 was assayed in rats and NOS-I knockout mice, and PET was performed in baboons. Tracer kinetic modeling used a 2-compartment plasma and brain tissue model. **Results:** Yields of [^{11}C]AR-R 17443 and [^{11}C]AR-R 18512 ranged from 8% to 16% at the end of synthesis, with specific activities of 50–178 GBq/ μmol (1350–4800 Ci/mmol) at the end of synthesis. In rat cerebellum and cortex at 30 min after injection, [^{11}C]AR-R 17443 showed 1.01 ± 0.01 and 1.63 ± 0.12 percentage injected dose per gram (%ID/g) uptake, respectively, whereas [^{11}C]AR-R 18512 showed 0.88 ± 0.01 and 1.30 ± 0.07 %ID/g uptake, respectively. Attempts to block tracer uptake by pretreatment with the NOS-I-selective inhibitor 7-nitroindazole or the corresponding unlabeled inhibitor (or desmethyl precursor to AR-R 17443 of similar potency) were unsuccessful. A small but significant (20%) decrease in cerebellar uptake of [^{11}C]AR-R 18512 was present in NOS-I knockout mice compared with control mice. PET of [^{11}C]AR-R 18512 in baboons with concurrent regional cerebral blood flow (rCBF) determination before and after administration of blocker showed dose-related decreases in cerebellar uptake that were greater than or equal to decreases in rCBF. Plasma metabolites accounted for 27% of total activity at 30 min after injection. Kinetic modeling of binding potentials revealed a distribution volume of 334 in cerebral blood that dropped 51% after blocker administration. **Conclusion:** Rodent studies for [^{11}C]AR-R 17443 and [^{11}C]AR-R 18512 showed little evidence of specific NOS-I binding. In baboons, we detected a higher uptake of [^{11}C]AR-R 18512 in the cerebellum than in the cortex (approximately 5%, accounting for decreased rCBF because of blockade), indicating minimal specific binding. Analogs of higher affinity are likely required if this class of agents is to prove viable for PET.

Key Words: thiopheneamidine; nitric oxide synthase; knockout mice; baboon; PET

J Nucl Med 2000; 41:1417–1425

Nitric oxide synthase (NOS) converts L-arginine to L-citrulline and its coproduct nitric oxide (NO) in a 5-electron oxidation process (1). Three isoforms of NOS exist and are historically differentiated on the basis of their respective cell or tissue of residence; however, they may be labeled unambiguously NOS-I, NOS-II, and NOS-III, reflecting the order in which they were discovered (2). NOS-I (neuronal) and NOS-III (endothelial) are low-output isoforms, producing NO constitutively. NO derived from NOS-I and NOS-III is a mediator of signal transduction. From NOS-I, NO may act as a neurotransmitter (3), engender synaptic plasticity (4), promote excitotoxicity (5), or effect changes in regional cerebral blood flow (rCBF) during brain activation (6). Alternative splice variants of NOS-I exist, each with a different function, with the major isoform important in development of morphine tolerance and a minor isoform facilitating morphine analgesia (7). NOS-III-derived NO modulates vascular tone (8). NOS-II (inducible), the high-output isoform, resides in macrophages, is induced by cytokines, and may behave as a bactericidal or tumoricidal agent (9).

Because of the ubiquity of NOS, the ability to assess its activity in vivo could provide insight into a wide variety of physiologic and pathologic processes. Isoform-selective NOS imaging would be particularly desirable, because the relative contribution of the various isoforms to certain pathologic and physiologic processes in vivo remains unclear. Differences in metabolism between amino acid analog inhibitors (10) and between the L-arginine binding site of the constitutive NOS isoforms and NOS-II indicate that isoform-selective inhibitors can be synthesized, and several groups of investigators have done precisely that (11–14). That the crystal structure for NOS-II has recently been solved suggests that even more selective inhibitors may be realized

Received Aug. 9, 1999; revision accepted Nov. 2, 1999.

For correspondence or reprints contact: Martin G. Pomper, MD, PhD, Division of Neuroradiology, Johns Hopkins University School of Medicine, 600 N. Wolfe St., Baltimore, MD 21287-2182.

(15). Several positron-emitting NOS inhibitors have recently been produced, 2 of which display a certain degree of isoform selectivity (16–18). Our goals were to synthesize NOS-I-selective imaging agents in positron-emitting form and to evaluate their regional brain uptake in rodents and primates. The agents we chose were based on a series of thiopheneamidines recently developed at Astra Arcus U.S.A., Rochester, NY (19,20). NOS-I knockout mice (21) were used to help evaluate isoform selectivity.

MATERIALS AND METHODS

Chemistry

N,N-dimethylformamide was distilled under reduced pressure from BaO. High-performance liquid chromatography (HPLC) equipment consisted of model 7126 injectors (Rheodyne, Rohnert, CA), model 590 EF pumps (Waters, Milford, MA), a model 440 ultraviolet absorbance detector (254 nm) (Waters), and a 5.08-cm (2-in.) NaI(Tl) crystal scintillation detector (model 276; Ortec, Oak Ridge, TN). Model 3390A integrators (Hewlett-Packard, Andover, MA) and a Dynamax system (Rainin Instrument Co., Woburn, MA) were used to record and analyze HPLC chromatograms. Semi-preparative (10 × 250 μm) and analytical (4.6 × 250 mm) reverse-phase HPLC columns (Econosil C₁₈, 10 mm; Alltech Associates, Inc., Deerfield, IL) were used for purification and quality control, respectively, of the radiotracers. Syntheses of AR-R 17443 and AR-R 18512 have been previously described (19,20). The desmethyl precursors of those compounds were synthesized by analogous techniques. AR-R 17443 and AR-R 18512 possess K_i (nanomole per liter) values of 10 and 40, respectively, for NOS-I and selectivity ratios (in vitro) of 80 and 440, respectively for NOS-I/NOS-II. The K_i values for the NOS isozymes were determined according to methods previously described (22).

For preparation of [¹¹C]AR-R 17443 (Fig. 1), [¹¹C]iodomethane, carried by a stream of nitrogen, was trapped in a solution of the desmethyl precursor (0.5–1.0 mg) in *N,N*-dimethylformamide (0.2 mL) cooled with dry ice and ethanol. The reaction was heated at 80°C for 3 min before quenching with 200 μL HPLC mobile phase consisting of 40:60 acetonitrile:water in 0.1 mol/L ammonium formate. The crude reaction was purified by reverse-phase HPLC using the same mobile phase at 10 mL/min. The radioproduct (radiologic half-life [t_R] = 6.4 min; k' = 5.9), which was well

separated from the precursor (t_R = 2.2 min; k' = 1.4), was remotely collected. After concentration to dryness under reduced pressure and heat (80°C), the radiotracer was reconstituted in sterile 0.9% saline (7.0 mL) and passed through a 0.2-μm sterile filter (Acrodisc; Pall Gelman Laboratory, Ann Arbor, MI) into a sterile, pyrogen-free multidose vial. Sterile NaHCO₃ (3.0 mL, 8.4%) was added to give a final formulation of pH 7.4. An aliquot (100 μL) was assayed for radioactivity and checked by analytic HPLC using a mobile phase of 60:40 acetonitrile:water in 0.1 mol/L ammonium formate at 6 mL/min. A single radioactive peak (t_R = 1.6 min; k' = 1.7) corresponding to authentic AR-R 17443 was observed. Specific radioactivity was calculated by relating radioactivity to the mass associated with the ultraviolet absorbance peak of the carrier. Specific radioactivities ranged from 50 to 70 GBq/μmol (1350–1900 Ci/mmol), with an average (n = 4) of 57 GBq/μmol (1530 Ci/mmol) calculated at the end of synthesis.

In a similar manner, [¹¹C]AR-R 18512 (Fig. 1) was prepared by reacting [¹¹C]iodomethane with the desmethyl precursor (1.0 mg) in DMF (0.2 mL). The reaction was heated at 80°C for 3 min before quenching with 200 μL HPLC mobile phase consisting of 25:75 acetonitrile:water in 0.1 mol/L ammonium formate. The crude reaction was purified by reverse-phase HPLC using the mobile phase at 8 mL/min. The radioproduct (t_R = 4.2 min), which was resolved from the precursor (t_R = 2.5 min), was collected remotely. The radiotracer was formulated in the same manner as for [¹¹C]AR-R 17443. Specific radioactivities, calculated in a manner identical to that for [¹¹C]AR-R 17443, ranged from 130 to 178 GBq/μmol (3500–4800 Ci/mmol), with an average (n = 6) of 153 GBq/μmol (4130 Ci/mmol) calculated at the end of synthesis. The average radiochemical yield was 9.8% non-decay corrected. The time for synthesis, including formulation, was approximately 18 min.

Animal Studies

Rodent In Vivo Biodistribution Studies of [¹¹C]AR-R 17443 and [¹¹C]AR-R 18512. All animal studies were approved by the Animal Care and Use Committee of the Johns Hopkins University. Male Sprague-Dawley rats (Charles River, Wilmington, MA) weighing between 200 and 250 g were used and received an injection of 18.5 MBq (500 μCi) of either [¹¹C]AR-R 17443 or [¹¹C]AR-R 18512 through the tail vein. The corresponding amounts were approximately 0.4 μg/kg and 0.3 μg/kg, respectively. For kinetic studies, the rats were killed by cervical dislocation at 15, 30, and 60 min after intravenous injection of radiotracer in 1 mL saline vehicle.

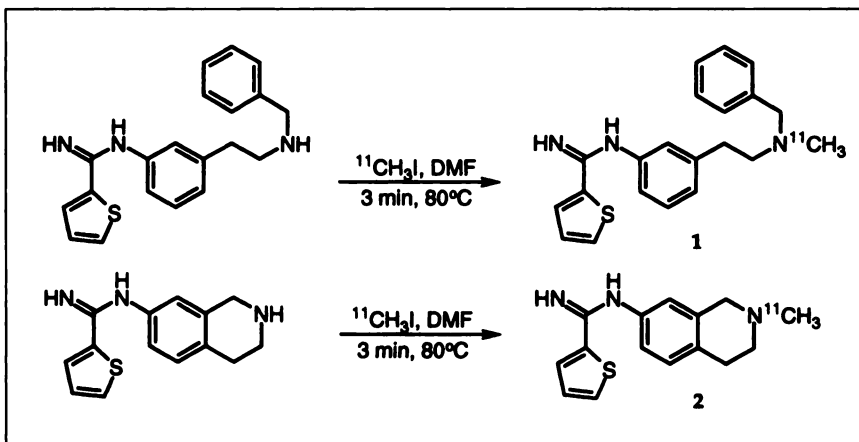


FIGURE 1. Syntheses of [¹¹C]AR-R 17443 (1) and [¹¹C]AR-R 18512 (2).

The brains were removed and placed on ice, and the cerebellum, olfactory bulb, hypothalamus, hippocampus, striatum, cortex, brain stem, and thalamus were harvested. Blood and fat were also harvested. The tissue samples were weighed, and their radioactivity content was determined in an automated γ counter (1282 Compu-gamma CS; Pharmacia/LKB Nuclear Inc., Gaithersburg, MD). Aliquots of the injected tracer were counted along with the samples and served as standards for the calculation of percentage injected dose per gram of tissue (%ID/g). To assess binding specificity, subgroups of rats were treated with the NOS-I-specific inhibitor 7-nitroindazole (23) (40 mg/kg intraperitoneally in arachis oil) 30 min before injection of radiotracer ($[^{11}\text{C}]\text{AR-R 17443}$ or $[^{11}\text{C}]\text{AR-R 18512}$), which occurred 60 min before the rats were killed. Other subgroups received either AR-R 16936, the equipotent desmethyl precursor to AR-R 17443 (10 mg/kg intravenously in acidified saline [pH 4]), or AR-R 18512 (20 mg/kg intravenously in saline) 1 h before injection of $[^{11}\text{C}]\text{AR-R 17443}$ or $[^{11}\text{C}]\text{AR-R 18512}$, respectively, which occurred 90 min before the rats were killed. For enhancement of NOS-I activity, another subgroup of rats received *N*-methyl-D-aspartate (NMDA) (50 mg/kg intraperitoneally in saline) 30 min before the radiotracer ($[^{11}\text{C}]\text{AR-R 17443}$ or $[^{11}\text{C}]\text{AR-R 18512}$) and were killed an additional 30 min later.

NOS-I knockout mice (28–30 g) were provided by Mikael Eliasson (Johns Hopkins University). SV 129 (25–29 g) and C57/BL-6 (24–26 g) mice (Taconic Farms, Inc., Germantown, NY) served as controls (24) for the radiotracer uptake experiment. The mice were injected with 7.4 MBq (200 μCi) $[^{11}\text{C}]\text{AR-R 18512}$ through the tail vein and were killed by cervical dislocation either 15 min or 60 min later. The brains were removed and placed on ice, and the cerebellum, olfactory bulb, cortex, and brain stem were harvested, weighed, and counted for radioactivity as described for the rats. The %ID/g tissue values were corrected for individual animal weights.

Baboon PET Studies of $[^{11}\text{C}]\text{AR-R 17443}$ and $[^{11}\text{C}]\text{AR-R 18512}$. Four PET studies of the brain distribution of $[^{11}\text{C}]\text{AR-R 18512}$ and 1 PET study of $[^{11}\text{C}]\text{AR-R 17443}$ were performed in adult male baboons (*Papio anubis*; body weight, approximately 30 kg). Quantitative measurement of rCBF using $[^{15}\text{O}]\text{H}_2\text{O}$ was performed concurrently for each animal (25). Before each study, 2 intravenous catheters and a single arterial catheter were placed for infusion of anesthesia, injection of radiotracer, and sampling of arterial blood, respectively. The animals were initially anesthetized intramuscularly with 8–10 mg/kg alfadolone and alfalone acetate (Saffan; Pitman-Moore, Middlesex, UK) and intubated. Anesthesia was maintained throughout the study by a continuous intravenous infusion drip of 6–9 mg/kg/h Saffan. The animals were secured to the PET bed using an individually fitted thermoplastic mask that allowed reproducible positioning between studies, as necessary. Pulse, blood pressure, and oxygen saturation were monitored continuously during the studies. Blood oxygen saturation was always maintained above 85%. After the animals were positioned in the PET scanner, transmission scanning was performed with a 370-MBq (10 mCi) ^{68}Ga source to allow for attenuation correction. PET scanning was started immediately after intravenous injection of 740–1110 MBq (20–30 mCi) high-specific-activity $[^{11}\text{C}]\text{AR-R 17443}$ or $[^{11}\text{C}]\text{AR-R 18512}$ (corresponding to approximately 0.09 $\mu\text{g/kg}$). Fifteen simultaneous, contiguous (8 direct planes, 7 cross planes, z-axis = ~ 10 cm), sequential, quantitative tomographic slices of the brain were obtained with a model 4096+ PET tomograph (General Electric Medical Systems, Milwaukee, WI) in the high-resolution mode (~ 6.5 mm full width at half maximum),

over a 90-min period. The animals were positioned so that the lowest plane was approximately 5 cm below the canthomeatal line. Approximately 30 arterial samples per PET study (for radioassay and protein binding) were obtained over 90 min. To correct the input function for unmetabolized $[^{11}\text{C}]\text{AR-R 17443}$ or $[^{11}\text{C}]\text{AR-R 18512}$, arterial samples were also obtained at 5, 12, 30, 50, and 75 min after injection of the radiotracer for analysis by HPLC. In the column-switch HPLC method, 4 mL plasma were loaded at 2 mL/min onto a capture column measuring 4.6×19.0 mm packed with C_{18} SepPak (Waters) stationary phase. Washing the capture column with 1% acetonitrile for an additional 2 min flushed plasma proteins from the system. The parent compound and moderately polar metabolites were quantitatively retained by the capture column. Highly polar metabolites failed to bind and passed through the capture column to the detector, from which the radioactivity was recorded as a broad radioactive peak representing the 4-mL sample load. Four minutes after the sample injection, the analytic solvent (40% acetonitrile in 100 mmol/L triethylamine acetate, pH 4.1) was switched to back-flush the contents of the capture column (1 mL/min) onto the analytic column (ABZ+, 4.6×250 mm; Supelco, Bellefonte, PA), where chromatography of the parent compound and moderately polar metabolites occurred. Radioactivity detected by a sodium iodide detector was recorded and integrated by Dynamax HPLC software (Rainin Instrument Co.).

PET images were reconstructed from the raw data with a standard filtered backprojection algorithm and a Hanning filter (6.0 mm). Images were corrected for attenuation and decay and were scaled to the same maximum. With reference to a baboon PET atlas (26), regions of interest were placed manually over the cortex, cerebellum, and brain stem, and time-activity curves (TACs) were generated. To assess binding specificity, 1–3 mg/kg of either AR-R 16936 (in the case of $[^{11}\text{C}]\text{AR-R 17443}$) or AR-R 18512 (in the case of $[^{11}\text{C}]\text{AR-R 18512}$) were administered intravenously for 75 min through a Harvard pump (Harvard Apparatus, Inc., Holliston, MA) at the end of the first 90-min scan. A second radiotracer ($[^{11}\text{C}]\text{AR-R 17443}$ or $[^{11}\text{C}]\text{AR-R 18512}$) injection immediately followed infusion of the corresponding unlabeled inhibitor, and scanning proceeded as before. Quantitative rCBF values were obtained 15 min before and 15 min after infusion of the unlabeled inhibitor. For rCBF determinations, a 90-s scan was obtained and blood radioactivity levels were concurrently measured by an automated blood sampling system. Regions of interest identical to those for $[^{11}\text{C}]\text{AR-R 17443}$ and $[^{11}\text{C}]\text{AR-R 18512}$ were used to generate TACs.

Tracer Kinetic Modeling

A 2-compartment plasma and brain tissue model was applied to the TACs and to the brain and plasma metabolite-corrected curves. Individual rate constants for the forward and reverse plasma-to-brain rate constants, K_1 and k_2 , and a blood volume term were obtained. Other methods, including a 3-compartment tissue model, were found to be less robust. The kinetic modeling chosen was similar to that of Koeppe et al. (27). In this 2-compartment model, the ratio of K_1/k_2 is considered to be an estimate of the distribution volume (V_D , in milliliters per gram) and proportional to the binding potential, V_{max}/K_m ; however, as has been found for several other radiotracers (28), the free and bound brain tissue compartments could not easily be separated. Hence, this method was chosen as containing the most information and being the most appropriate model.

The plasma input was corrected with plasma metabolites

detected by HPLC. The model was fit to the PET data using nonlinear least squares minimization (29). The V_D was expressed as K_1/k_2 and provided independent estimates of tracer delivery and binding (27).

Statistics

ANOVA, which was used in rodent radiotracer uptake studies, was performed with StatView SE + Graphics software, version 1.03 (SAS Institute, Cary, NC). For the Scheffé procedure, the Fisher test of protected least significant difference, and the Student *t* test, $P < 0.05$ was considered to indicate statistical significance.

LogD_{7.4} Values

LogD_{7.4} values were calculated using ACD/Pka DB software, version 3.00 (Advanced Chemistry Development Inc., Toronto, Ontario, Canada).

RESULTS

Radiochemical Syntheses

Facile radiosynthesis of thiopheneamidines [¹¹C]AR-R 17443 and [¹¹C]AR-R 18512 was effected by treatment of the corresponding desmethyl precursors with [¹¹C]iodomethane as depicted in Figure 1. Yields ranged from 8% to 16% (end of synthesis), with specific activities of 50–166 GBq/μmol (1350–4500 Ci/mmol). The total synthesis time was approximately 20 min.

Rodent Brain Biodistribution Studies

Regional brain uptake at 15, 30, and 60 min for [¹¹C]AR-R 17443 and [¹¹C]AR-R 18512 in rats is presented in Tables 1 and 2, respectively. Radiotracer uptake was higher in the cortex than in the cerebellum for both compounds. Pretreatment of animals with the in vivo NOS-I-selective inhibitor 7-nitroindazole (23) effected a decrease in radiotracer uptake in the striatum and cortex for [¹¹C]AR-R 17443 and in the cortex for [¹¹C]AR-R 18512. For neither radiotracer, however, was decreased uptake observed in the target areas (i.e., the olfactory bulb and cerebellum), which were brain regions with known high NOS-I activity (Figs. 2 and 3; Scheffé procedure) (30). Pretreatment with NMDA significantly inhibited uptake in the hippocampus, striatum, and cortex for [¹¹C]AR-R 17443 and [¹¹C]AR-R 18512 (Figs. 2

TABLE 2
Biodistribution of [¹¹C]AR-R 18512 in Male
Sprague-Dawley Rats

Tissue	%ID/g ± SD (n = 3)		
	5 min	30 min	60 min
Blood	0.03 ± 0.00	0.02 ± 0.00	0.02 ± 0.00
Cerebellum	0.60 ± 0.04	0.58 ± 0.05	0.63 ± 0.03
Olfactory bulb	0.71 ± 0.06	0.67 ± 0.06	0.76 ± 0.04
Hippocampus	0.50 ± 0.10	0.49 ± 0.05	0.60 ± 0.04
Cortex	0.89 ± 0.12	0.88 ± 0.07	1.00 ± 0.04
Brain stem	0.53 ± 0.04	0.53 ± 0.05	0.52 ± 0.02

Each rat received approximately 18.5 MBq (500 μCi [0.38 μg]) [¹¹C]AR-R 18512. Data are mean ± SD.

and 3; Scheffé procedure). The insets to Figures 2 and 3 indicate brain uptake in the cortex and cerebellum in rats pretreated with either AR-R 16936, the desmethyl precursor to AR-R 17443 (for [¹¹C]AR-R 17443), or AR-R 18512 (for [¹¹C]AR-R 18512), respectively. No blocking of radiotracer uptake for either compound was shown in either brain region.

Brain uptake of [¹¹C]AR-R 18512 was evaluated in NOS-I knockout mice (Fig. 4). A trend toward lower uptake in all investigated brain regions was shown in the knockout mice relative to the wild-type animals. That trend reached statistical significance (Fisher test) in the cerebellum at 15 min when the knockout mice were compared with 1 wild-type strain (SV-129) and at 60 min when the knockout mice were compared with the other wild-type strain (C57-BL/6).

PET

When [¹¹C]AR-R 18512 was administered to baboons, uptake was identified diffusely within the cortex and to a greater extent within the cerebellum (Fig. 5). Radiotracer uptake was also seen in the region of the pituitary and within the nasopharyngeal mucosa. Pretreatment with 3 mg/kg AR-R 18512 diminished uptake in the brain but also within the nasopharynx. Metabolites accounted for 27% of total activity at 30 min after injection, with 1 metabolite more lipophilic than AR-R 18512. In Figure 6, the preblockade TACs for the cerebellum and cortex (inset) for [¹¹C]AR-R 18512 depict the approximately 15% greater uptake in target tissue (cerebellum). A similar brain distribution for [¹¹C]AR-R 17443 (cerebellum > cortex) was also shown in 1 experiment using a rhesus monkey (Pomper et al., unpublished data, 1997). TACs for the cerebellum and cortex (inset) in Figure 6 also portray the degree of NOS-I blockade brought about by pretreatment (1.5 mg/kg AR-R 18512). The effect of pretreatment was approximately 15% greater in the cerebellum than in the cortex.

To learn whether the lower radiotracer uptake of [¹¹C]AR-R 18512 after pretreatment with a blocking dose of AR-R 18512 indeed resulted from competitive inhibition, we examined the effects of nonradiotracer doses of AR-R 18512 on blood flow in concurrent quantitative rCBF studies using

TABLE 1
Biodistribution of [¹¹C]AR-R 17443 in Male
Sprague-Dawley Rats

Tissue	%ID/g ± SD (n = 3)		
	5 min	30 min	60 min
Blood	0.03 ± 0.00	0.03 ± 0.00	0.02 ± 0.00
Cerebellum	0.72 ± 0.04	0.79 ± 0.08	0.88 ± 0.10
Olfactory bulb	1.01 ± 0.15	1.01 ± 0.08	0.96 ± 0.37
Hippocampus	0.70 ± 0.10	0.73 ± 0.09	0.77 ± 0.16
Cortex	1.34 ± 0.25	1.29 ± 0.22	1.56 ± 0.23
Brain stem	0.64 ± 0.06	0.78 ± 0.08	0.86 ± 0.09

Each rat received approximately 18.5 MBq (500 μCi [0.84 μg]) [¹¹C]AR-R 17443. Data are mean ± SD.

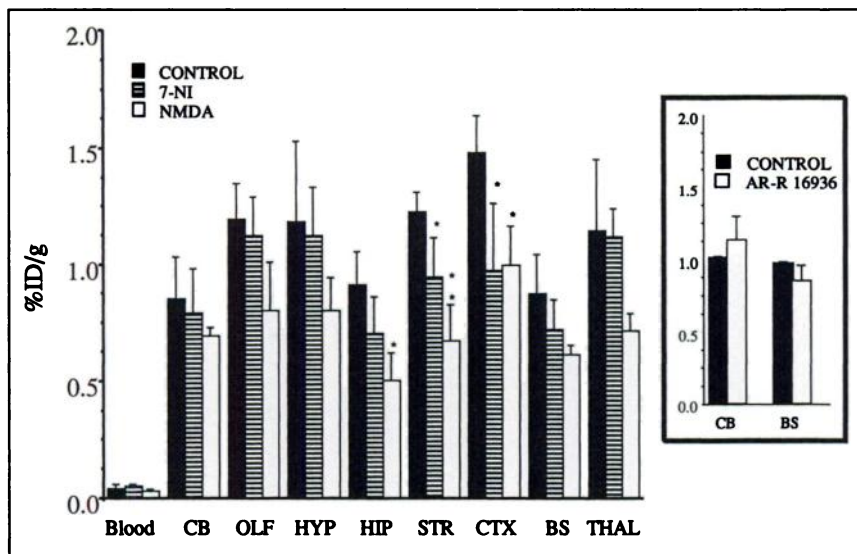


FIGURE 2. Regional uptake of [^{11}C]AR-R 17443 in male Sprague-Dawley rats. Control animals and animals treated with 7-nitro-indazole (7-NI) and NMDA were studied. Rats treated with 7-NI showed significant decreases in uptake in striatum (STR) and cortex (CTX). Rats treated with NMDA showed significant decreases in hippocampus (HIP), striatum, and cortex. Inset shows no blocking in cerebellum (CB) or brain stem (BS) when rats were pretreated with AR-R 16936, an equipotent NOS-I inhibitor to AR-R 17443. Results are expressed as mean \pm SD; $n = 3$. HYP = hypothalamus; OLF = olfactory bulb; THAL = thalamus.

[^{15}O]H $_2$ O (Fig. 7). Although cortical rCBF changes were not different, a significant difference (t test) of 10% was shown in the cerebellum. Although data for only 1 baboon are presented, similar results were seen in 3 additional studies, which used 2 other baboons and several doses of AR-R 18512 for pretreatment. Only 1 baboon study involved AR-R 17443 pretreatment and uptake of [^{11}C]AR-R 17443, again with little evidence of specific binding.

Tracer Kinetic Modeling

Tracer kinetics were modeled for [^{11}C]AR-R 18512 to define better whether any specific binding was present or whether [^{11}C]AR-R 18512 behaved merely as a perfusion tracer. A 3-compartment model was initially attempted; however, neither a k_3 nor a k_4 was identifiable. The fitting of V_D to a 2-compartment, 1-tissue model is presented in Table 3. The V_D s were large—in the range of 300–900 in the unblocked state and falling to 150–250 in the blocked state.

That finding was likely caused by the relatively fast dissociation (low k_2) observed in the modeling fits to all brain regions. However, the fits to all brain regions were excellent and had root mean square errors of approximately 0.05–0.15. Thus, a substantial decrease in V_D has been shown after preadministration of the inhibitors, with excellent fitting to both preblockade and postblockade brain TACs.

DISCUSSION

Imaging agents based on the thiopheneamides AR-R 17443 and AR-R 18512 are attractive candidates for NOS-I imaging because they are relatively selective for NOS-I in comparison with the other isoforms, they readily cross an intact blood–brain barrier, and they are easily synthesized in ^{11}C labeled form. The affinities of [^{11}C]AR-R 17443 and [^{11}C]AR-R 18512 ($K_i = 10$ and 40 nmol/L, respectively) are somewhat marginal, particularly considering that the active

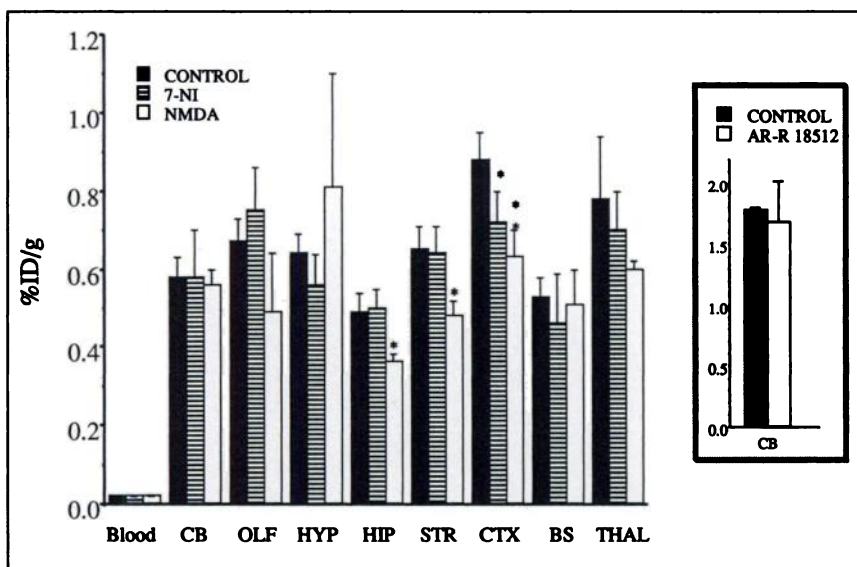
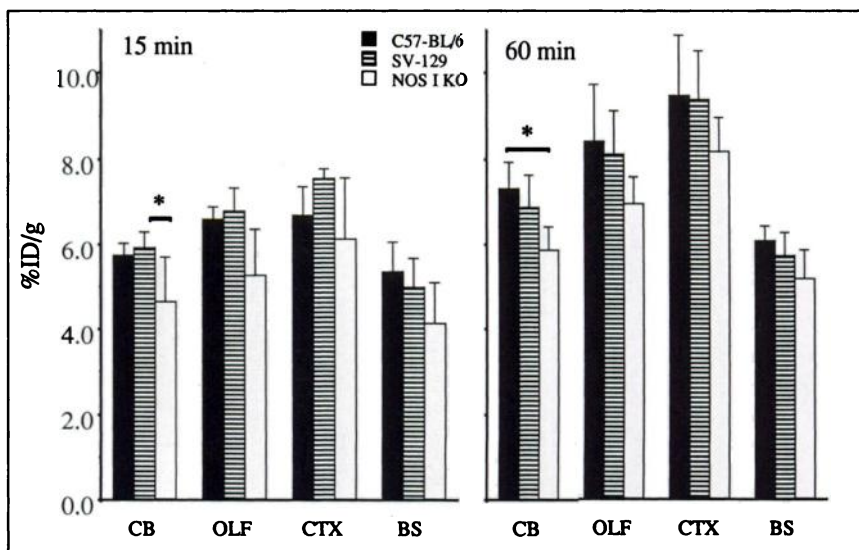


FIGURE 3. Regional uptake of [^{11}C]AR-R 18512 in male Sprague-Dawley rats. Control animals and animals treated with 7-nitro-indazole (7-NI) and NMDA were studied. Rats treated with 7-NI showed significant decreases in uptake in cortex (CTX). Rats treated with NMDA showed significant decreases in hippocampus (HIP), striatum (STR), and cortex. Inset shows no blocking in cerebellum (CB) when rats were pretreated with AR-R 18512. Results are expressed as mean \pm SD; $n = 3$. BS = brain stem; HYP = hypothalamus; OLF = olfactory bulb; THAL = thalamus.

FIGURE 4. Regional brain uptake of [^{11}C]AR-R 18512 in NOS-I knockout, C57-BL/6, and SV-129 mice. Significant decreases in uptake are noted in cerebellum (CB) between knockout (KO) mice and SV-129 (15 min) and C57-BL/6 (60 min) mice. BS = brain stem; CTX = cortex; OLF = olfactory bulb.



site of NOS-I is nearly continuously saturated by its natural substrate, L-arginine ($K_m = 1.5\text{--}2.2\text{ }\mu\text{mol/L}$) (2). Radiosynthesis of [^{11}C]AR-R 17443 and [^{11}C]AR-R 18512 proceeded efficiently, and in high specific radioactivities, through N-alkylation of the highly nucleophilic secondary amine. The specific activity of [^{11}C]AR-R 18512 was consistently more than double that of [^{11}C]AR-R 17443. Although the reason for that result is unclear, the specific activities were high enough in each case to obtain reliable biologic results.

That [^{11}C]AR-R 17443 and [^{11}C]AR-R 18512 gain substantial access to the brain is evident by the moderate brain uptake values shown in Tables 1 and 2. That [^{11}C]AR-R 17443 displays somewhat higher brain uptake in all tissues and at all times investigated may reflect the higher octanol-buffer partition coefficient ($\log D_{7.4}$) for [^{11}C]AR-R 17443 (2.56) relative to [^{11}C]AR-R 18512 (0.57). Detection of little radioactivity in the blood indicates few polar radiolabeled

metabolites. Similarly, low levels of radioactivity were detected in fat (Pomper et al. unpublished data, 1997). For both compounds, the brain region displaying the highest uptake was the cortex, a finding not in accordance with the known distribution of NOS-I in rat brain, in which olfactory bulb and cerebellar levels are about 6-fold greater than cortical levels (30–32).

Figures 2 and 3 indicate the low tissue selectivity of [^{11}C]AR-R 17443 and [^{11}C]AR-R 18512, respectively, for rat brain. In addition to inhibiting NOS-I, 7-nitroindazole is known to decrease rCBF in a region-specific manner (33,34), perhaps accounting for lower radiotracer uptake in certain regions. Pretreatment with NMDA in an effort to upregulate NOS-I activity (35) and possibly increase radiotracer uptake in target areas merely led to decreased uptake in the hippocampus, striatum, and cortex for [^{11}C]AR-R 17443 and [^{11}C]AR-R 18512. Decreased uptake may have been caused

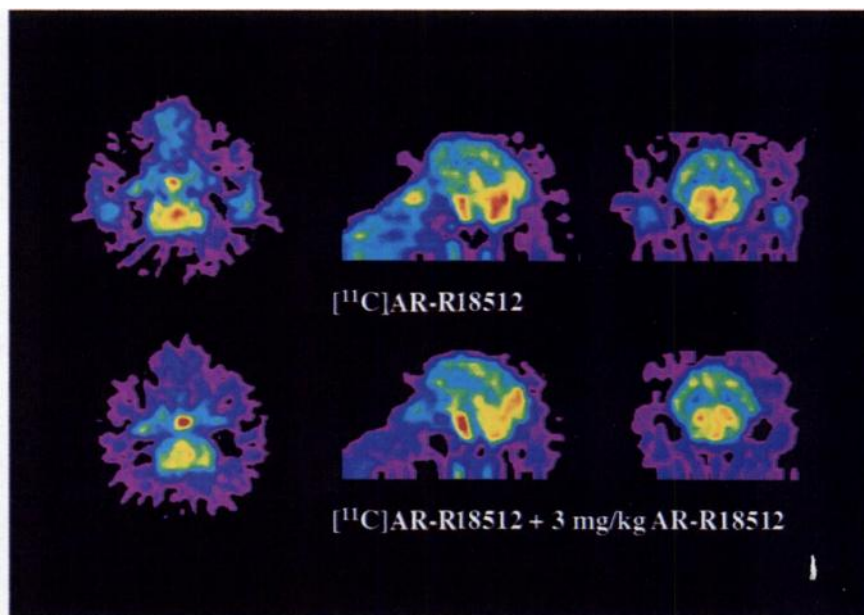


FIGURE 5. PET images with [^{11}C]AR-R 18512 in baboon. Top row was obtained before blockade with AR-R 18512; bottom row was obtained after blockade (1.04 GBq [28 mCi] [^{11}C]AR-R 18512; specific activity = 97.6 GBq/ μmol [2635 Ci/ mmol]). Left to right: axial, sagittal, and coronal images.

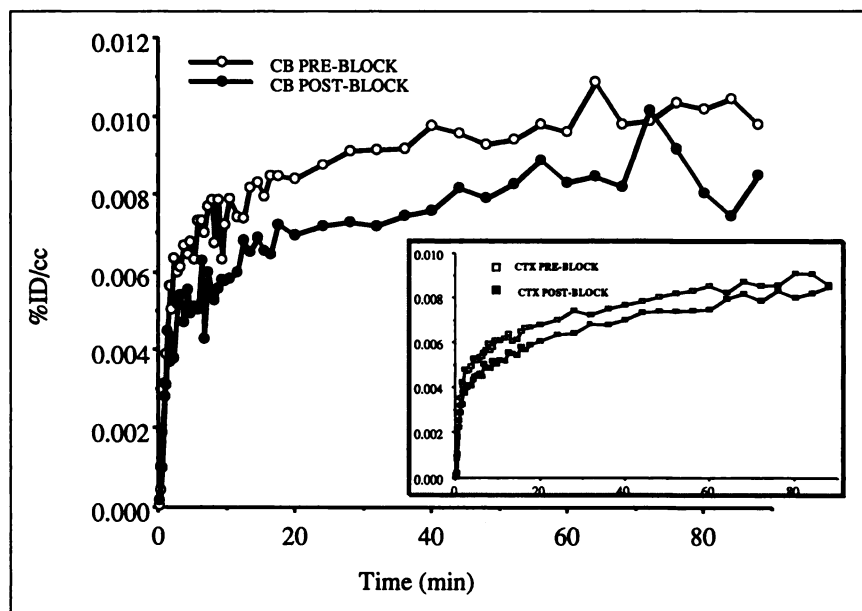


FIGURE 6. Cerebellum (CB) TACs for [^{11}C]AR-R 18512 before and after blockade with AR-R 18512 (1.5 mg/kg). Inset shows cortex (CTX) TAC for [^{11}C]AR-R 18512 before and after blockade.

by an acute cytotoxic effect of NMDA on those brain regions, each of which is particularly vulnerable to such excitotoxic injury (36), with a consequent decrease in rCBF. The insets to Figures 2 and 3, which describe attempts at self-blockade of the enzyme before radiotracer injection, further indicate the lack of NOS-I-specific binding of either [^{11}C]AR-R 17443 or [^{11}C]AR-R 18512. The need to use blocking agents that affect rCBF in showing specific binding for NOS-I renders such experiments difficult to interpret. One way to circumvent the effect of rCBF alterations on radiotracer delivery is concurrent measurement of rCBF. Alternatively, knockout mice, lacking the enzyme of interest, may be used.

Transgenic or knockout mice have not been used fre-

quently in radiopharmaceutical development, but their potential for use is vast as increasingly selective targets are pursued. However, such mice are being increasingly used in nuclear medicine to study noninvasively the physiologic effects of genetic alteration (37,38). For all brain regions, NOS-I knockout mice showed merely a trend toward decreased uptake of radioactivity relative to control mice (Fig. 4); the only area of significantly decreased uptake was the cerebellum. That the cerebellum is a NOS-I target tissue suggests that a portion of radiotracer uptake in the wild-type animals may be caused by specific binding. The greater overall radioactivity levels at 60 min relative to 15 min reflects the fact that equilibrium has not yet been achieved by this radiotracer, a finding that correlates with the baboon

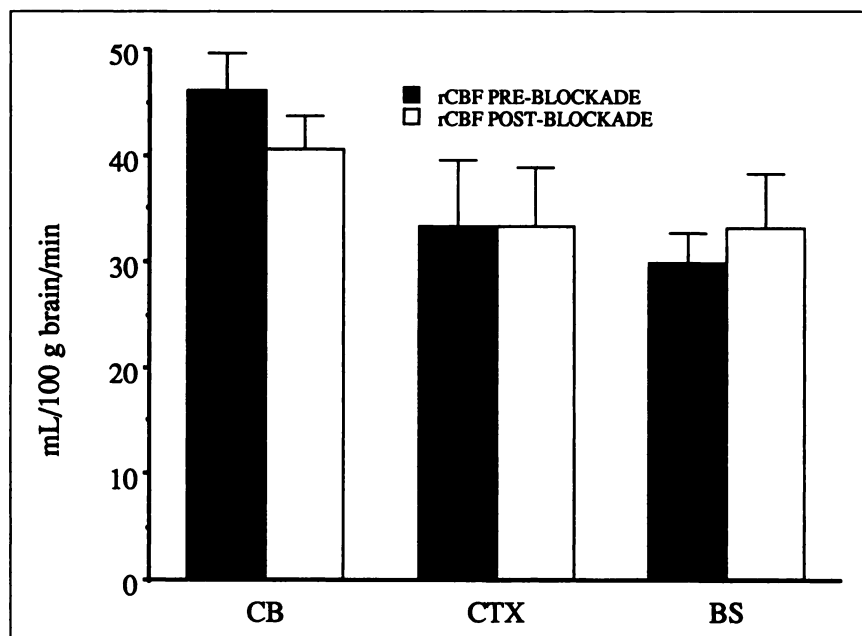


FIGURE 7. Regional effect of blockade (AR-R 18512, 1.5 mg/kg) on rCBF. Small (~10%) but significant decrease in rCBF was noted in cerebellum (CB); no change was noted in cortex (CTX) or brain stem (BS).

TABLE 3
Distribution Volumes (K_1/k_2) of [^{11}C]AR-R 18512 Before
and After Blockade with AR-R 18512 (1.5 mg/kg)
in Baboon Brain

Region	K_1 (Before)	K_1 (After)	k_2 (Before)	k_2 (After)	K_1/k_2 (Before)	K_1/k_2 (After)
Cerebellum	0.537	0.526	0.0016	0.0032	334	165
Cortex	0.598	0.642	0.0007	0.0025	894	257
Brain stem	0.498	0.514	0.0011	0.0037	449	138

PET studies. Also notable is the substantially higher, nearly 6-fold, uptake of [^{11}C]AR-R 18512 in SV-129 and C57-BL/6 mice relative to rats, indicating a species difference. Higher radiolabeled NOS-inhibitor ([^3H]L-NNA) uptake in SV-129 mice relative to rats has been reported (39).

Unlike rodents, baboons showed a higher [^{11}C]AR-R 18512 uptake in the cerebellum than in the cortex (Figs. 5 and 6). Although this finding is superficially encouraging, NOS-I levels are known to be significantly higher in the cerebellum than in the cortex, and the known difference between these 2 regions is certainly more than the 15% difference we showed in radiotracer uptake (30–38). Furthermore, after pretreatment with AR-R 18512, the decreased nasopharyngeal uptake in an attempt at blockade militates against a specific mechanism for decreased radiotracer uptake (Fig. 5). For these reasons, the effect of various doses of AR-R 18512 (1–3 mg/kg) on rCBF, and hence radiotracer delivery, was investigated in detail. The results presented in Figure 7 indicate that a lower rCBF in the cerebellum accounts for most of the putative specific binding. [^{11}C]AR-R 18512 was pursued more vigorously than [^{11}C]AR-R 17443, despite the lower NOS-I inhibitory potency caused by the lower lipophilicity of AR-R 18512, because of its more tractable formulation medium and greater safety profile relative to AR-R 17443.

The results of V_D calculations using a metabolite-corrected plasma input function and fitted blood volume term indicate that a 1-tissue, 2-compartment model fit the data well in either preblockade or postblockade conditions. After treatment with a blocker, the V_D values (K_1/k_2) for [^{11}C]AR-R 18512 decreased by 50%–70% in all brain regions examined. Most of those changes were caused by increases in k_2 , i.e., washout. These results indicate that blocking induced increases in washout suggesting that this compound is not a pure perfusion tracer; however, the washout may have been from nonspecific brain sites as well as from NOS-I. These results are not corrected for a lipophilic brain metabolite identified on HPLC and do not account for the fact that the system has not yet achieved equilibrium.

Similar to the other report of a NOS-I-specific, positron-emitting radiopharmaceutical, [^{11}C]S-methyl-L-thiocitrulline (17), most of the radiotracer uptake that we showed was nonspecific. Unlike that other report, however, a significant degree of blockade was not shown in rodents. [^{11}C]AR-R

17443 and [^{11}C]AR-R 18512 readily access the primate brain, unlike [^{11}C]S-methyl-L-thiocitrulline. Nevertheless, the uptake seen is fraught with nonspecific binding caused by the relatively low affinities of [^{11}C]AR-R 17443 and [^{11}C]AR-R 18512 for NOS-I. Because high-affinity, low-lipophilicity L-arginine analogs such as S-methyl-L-thiocitrulline are transported across the blood–brain barrier through the γ^+ amino acid system (10), such compounds are promising for selective, potent NOS-I inhibition pharmacologically; however, they may suffer from pharmacokinetics that prevent access to NOS-I sites on a time-scale suitable for PET. Imaging agents directed toward other sites on NOS-I, such as the calmodulin binding site (40), may prove more suitable.

CONCLUSION

Positron-emitting analogs of the NOS-I-selective thiophenamidines AR-R 17443 and AR-R 18512 can be synthesized in moderate to high yields and in high specific radioactivity. Most binding of [^{11}C]AR-R 17443 and [^{11}C]AR-R 18512 was nonspecific in rodent and primate brain. To differentiate better between flow-mediated tracer delivery and specific binding, agents of this class require higher affinities and incorporation of a longer lived isotope to allow study under equilibrium conditions by PET.

ACKNOWLEDGMENTS

The authors thank Dr. John Hilton for metabolite analysis and Paige Finley, David Clough, and Karen Edmonds for technical assistance during the PET studies. This study was supported by the National Alliance for Research on Schizophrenia and Depression and the Radiological Society of North America Research and Education Fund.

REFERENCES

- Griffith OW, Stuehr DJ. Nitric oxide synthases: properties and catalytic mechanism. *Annu Rev Physiol*. 1995;57:707–736.
- Forstermann U, Gath I, Schwarz P, Closs EI, Kleinert H. Isoforms of nitric oxide synthase: properties, cellular distribution and expression control. *Biochem Pharm*. 1995;50:1321–1332.
- Dawson VL, Dawson TM. Nitric oxide actions in neurochemistry. *Neurochem Int*. 1996;29:97–110.
- Son H, Hawkins RD, Martin K, et al. Long-term potentiation is reduced in mice that are doubly mutant in endothelial and neuronal nitric oxide synthase. *Cell*. 1996;87:1015–1023.
- Dawson VL, Dawson TM. Nitric oxide neurotoxicity. *J Chem Neuroanat*. 1996;10:179–190.
- Cholet N, Bonvento G, Seylaz J. Effect of neuronal NO synthase on the cerebral vasodilatory response to somatosensory stimulation. *Brain Res*. 1996;708:197–200.
- Kolesnikov YA, Pan YX, Babey AM, Jain S, Wilson R, Pasternak GW. Functionally differentiating two neuronal nitric oxide synthase isoforms through antisense mapping: evidence for opposing NO actions on morphine analgesia and tolerance. *Proc Natl Acad Sci USA*. 1997;94:8220–8225.
- Faraci FM, Brian JE. Nitric oxide and the cerebral circulation. *Stroke*. 1994;25:692–703.
- Lowenstein CJ, Dinerman JL, Snyder SH. Nitric oxide: a physiologic messenger. *Ann Intern Med*. 1994;120:227–237.
- Babu BR, Griffith OW. N^5 -(1-imino-3-butenyl)-L-ornithine: a neuronal isoform selective mechanism-based inactivator of nitric oxide synthase. *J Biol Chem*. 1998;273:8882–8889.

11. Collins JL, Shearer BG, Oplinger JA, et al. *N*-phenylamidines as selective inhibitors of human neuronal nitric oxide synthase: structure-activity studies and demonstration of *in vivo* activity. *J Med Chem.* 1998;41:2858–2871.
12. Cowart M, Kowaluk EA, Daanen JF, et al. Nitroaromatic amino acids as inhibitors of neuronal nitric oxide synthase. *J Med Chem.* 1998;41:2636–2642.
13. Moore PK, Handy RLC. Selective inhibitors of neuronal nitric oxide synthase: is no NOS really good NOS for the nervous system? *Trends Pharm Sci.* 1997;18:204–211.
14. Southan GJ, Szabo C, O'Connor MP, Salzman AL, Thiemermann C. Amidines are potent inhibitors of nitric oxide synthases: preferential inhibition of the inducible isoform. *Eur J Pharm.* 1995;291:311–318.
15. Crane BR, Arvai AS, Ghosh DK, et al. Structure of nitric oxide synthase oxygenase dimer with pterin and substrate. *Science.* 1998;279:2121–2126.
16. Zhang J, McCarthy TJ, Moore WM, Curie MG, Welch MJ. Synthesis and evaluation of two positron-labeled nitric oxide synthase inhibitors, *S*-[¹¹C]methylisothioureia and *S*-2-[¹⁸F]fluoroethylisothioureia, as potential positron emission tomography tracers. *J Med Chem.* 1996;39:5110–5118.
17. Zhang J, Xu M, Dence C, Sherman ELC, McCarthy TJ, Welch MJ. Synthesis, *in vivo* evaluation and PET study of a carbon-11-labeled neuronal nitric oxide synthase (nNOS) inhibitor *S*-methyl-L-thiocitrulline. *J Nucl Med.* 1997;38:1273–1278.
18. Roeda D, Crouzel C, Brouillet E, Valette H. Synthesis and *in vivo* distribution of no-carrier-added *N*(ω)-nitro-L-arginine [¹¹C]methyl ester, a nitric oxide synthase inhibitor. *Nucl Med Biol.* 1996;23:509–512.
19. Gentile RT, Murray RJ, Macdonald JE, Shakespeare WC, inventors; AstraZeneca, assignee. Amidine derivatives with nitric oxide synthase activities. U.S. patent WO 9505363. February 12, 1995.
20. Macdonald JE, Matz JR, Shakespeare WC, inventors; AstraZeneca, assignee. Compounds. U.S. patent WO 9850380. November 12, 1998.
21. Huang PL, Dawson TM, Bredt DS, Snyder SH, Fishman MC. Targeted disruption of the neuronal nitric oxide synthase gene. *Cell.* 1993;75:1273–1286.
22. Reif DW, McCreedy SA. *N*-nitro-L-arginine and *N*-monomethyl-L-arginine exhibit a different pattern of inactivation toward the three nitric oxide synthases. *Arch Biochem Biophys.* 1995;320:170–176.
23. Babbedge RC, Bland-Ward PA, Hart SL, Moore PK. Inhibition of rat cerebellar nitric oxide synthase by 7-nitro indazole and related substituted indazoles. *Br J Pharmacol.* 1993;110:225–228.
24. Kano T, Shimizu-Sasamata M, Huang PL, Moskowitz MA, Lo EH. Effects of nitric oxide synthase gene knockout on neurotransmitter release *in vivo*. *Neuroscience.* 1998;86:695–699.
25. Meyer E. Simultaneous correction for tracer arrival delay and dispersion in CBF measurements by the H₂¹⁵O autoradiographic method and dynamic PET. *J Nucl Med.* 1989;30:1069–1078.
26. Riche D, Hantraye P, Guibert B, et al. Anatomical atlas of the baboon's brain in the orbito-meatal plane used in experimental positron emission tomography. *Brain Res Bull.* 1988;20:281–301.
27. Koeppel RA, Holthoff VA, Frey KA, Kilbourn MR, Kuhl DE. Compartmental analysis of [¹¹C]flumazenil kinetics for the estimation of ligand transport rate and receptor distribution using positron emission tomography. *J Cereb Blood Flow Metab.* 1991;11:735–744.
28. Frey KA, Koeppel RA, Mulholland GK, et al. *In vivo* muscarinic cholinergic receptor imaging in human brain with [¹¹C]scopolamine and positron emission tomography. *J Cereb Blood Flow Metab.* 1992;12:147–154.
29. Marquardt DW. An algorithm for least squares estimation on nonlinear parameters. *J Soc Ind Appl Math.* 1963;2:431–441.
30. Kidd EJ, Michel AD, Humphrey PPA. Autoradiographic distribution of [³H]L-NG-nitro-arginine binding in rat brain. *Neuropharmacology.* 1995;34:63–73.
31. Burazin TCD, Gundlach AL. Localization of NO synthase in rat brain by [³H]L-NG-nitro-arginine autoradiography. *Neuroreport.* 1995;6:1842–1844.
32. Arima T, Kitamura Y, Nishiyama T, Kiriya Y, Taniguchi T, Nomura Y. NG-nitro-L-[³H]arginine binding properties of neuronal nitric oxide synthase in rat brain. *Neurochem Int.* 1997;30:239–245.
33. Kelly PAT, Ritchie IM, Arbuthnott GW. Inhibition of neuronal nitric oxide synthase by 7-nitroindazole: effects upon local cerebral blood flow and glucose use in the rat. *J Cerebral Blood Flow Metab.* 1995;15:766–773.
34. Kalisch BE, Connop BP, Jhamandas K, Beninger RJ, Boegman, RJ. Differential action of 7-nitro indazole on rat brain nitric oxide synthase. *Neurosci Lett.* 1996;219:75–78.
35. Faraci FM, Brian JE. 7-Nitroindazole inhibits brain nitric oxide synthase and cerebral vasodilatation in response to *N*-methyl-D-aspartate. *Stroke.* 1995;26:2172–2176.
36. Lin B, Dietrich WD, Ginsberg MD, Globus MY, Busto R. MK-801 (dizocilpine) protects the brain from repeated normothermic global ischemic insults in the rat. *J Cereb Blood Flow Metab.* 1993;13:925–932.
37. Gambhir SS, Barrio JR, Phelps ME, et al. Imaging adenoviral-directed reporter gene expression in living animals with positron emission tomography. *Proc Natl Acad Sci USA.* 1999;96:2333–2338.
38. Pomper MG, Bhujwala ZM, Artemov D, et al. Measurement of [¹⁸F]fluorodeoxyglucose liver uptake in a c-myc transgenic mouse with positron projection imaging: a feasibility study. In: program and abstracts of High Resolution Imaging in Small Animals with PET, MR and Other Modalities (HiRes); September 27–29, 1999; Amsterdam, The Netherlands. Abstract 153.
39. Hara H, Waebler C, Huang PL, Fujii M, Fishman MC, Moskowitz MA. Brain distribution of nitric oxide synthase in neuronal or endothelial nitric oxide synthase mutant mice using [³H]L-NG-nitro-arginine autoradiography. *Neuroscience.* 1996;75:881–890.
40. Zoche M, Beyersmann M, Koch K-W. Introduction of a phosphate at serine⁷⁴¹ of the calmodulin-binding domain of the neuronal nitric oxide synthase (NOS-I) prevents binding of calmodulin. *Biol Chem.* 1997;378:851–857.